Hindawi
Advances in Civil Engineering
Volume 2019, Article ID 8987052, 10 pages
https://doi.org/10.1155/2019/8987052

Research Article

Experimental Study on the Permeability of a Soil-Rock Mixture Based on the Threshold Control Method

Xiaohua Ding[1,2] **Xuyang Shi**[1,2] **Wei Zhou**[1,2] **and Boyu Luan**[1,2]

[1]*School of Mines, China University of Mining and Technology, Xuzhou, Jiangsu 221116, China*
[2]*State Key Laboratory of Coal Resources and Safe Mining, China University of Mining and Technology, Xuzhou, Jiangsu 221116, China*

Correspondence should be addressed to Xuyang Shi; sxywlp2008@163.com

Received 25 October 2018; Revised 9 January 2019; Accepted 5 February 2019; Published 3 March 2019

Academic Editor: Flora Faleschini

The study of the permeability of soil-rock mixtures is important in supporting theories behind reclamation mechanisms for open-pit mines. To avoid the influence of differences in the spatial distribution of rock within the same sample on the permeability of a soil-rock mixture in laboratory tests, a numerical method for modelling the soil-rock mixture based on the threshold control method was proposed. Through the statistical results of 297 CT (computed tomography) cross sections of soil-rock mixture samples, the threshold values of pores, soils, and rocks are obtained, and a numerical model representing the reactions of the samples to real-world conditions is obtained. A numerical model was used that could vary with different rock block proportions (RBP) and porosities. Based on Darcy's law, it is concluded that macroscopic voids greatly increase the permeability of the sample due to their depth of penetration. The higher the stone content, the closer the permeability will be to the permeability of the rock skeleton. Therefore, during the reclamation process of the open-pit mine, the water-retaining layer below the humus should be compacted, and RBP should be increased to lower permeability and achieve better water retention.

1. Introduction

As China's environmental requirements improve, reclamation has become increasingly important in the area of open-pit mining. A waste dump is the main area of concern in open-pit mine reclamation and is composed of soil-rock mixtures produced by the mining process. To meet the water needs of plants, reclamation projects require a cover of humus and aquifers built into the topsoil. The hope is that the moisture of the humus soil and aquifer will not be lost, which means that the surface of the dump field must retain water [1–4], as is shown in Figure 1.

Therefore, studying the permeability of the rock aggregate within the dump is of great significance to reclamation work. However, the mesoscopic structure of the soil-rock mixture is very complicated. We hope to avoid incorporating error into the laboratory tests caused by differences in materials distribution in the sample, and a numerical simulation based on CT images is a suitable choice.

Numerical simulation based on digital images is an effective method to analyse the heterogeneity of materials, the characteristics of their internal structure, the characteristics of various components, and the corresponding mesoscopic properties. This method has achieved positive research results in analysing soil and stone mixtures as well as coal and concrete specimens.

Chen et al. [5] presented the background grid-EAB block casting algorithm and applied the manifold method in their simulation process, which simulates soil-rock mixture compression and verifies its effectiveness. Xu and Wang [6] tested a three-dimensional model of block stone. According to the test requirements, they built a soil and stone mixed model. They proved the rock-mass effect of the soil-rock mixture by simulating and combining test results. Liao et al. [7] simulated a uniaxial compression test based on a two-phase numerical model of soil and stone and concluded that stress in the specimen is affected by the distribution and shape of the stone. Meng et al. [8] proposed a method for generating a soil-rock mixture model and concluded that the

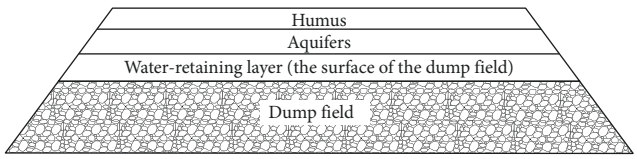

Figure 1: Reclaimed soil layer distribution in dumping field.

elastic modulus is positively correlated with model size and that the boundary effect is negatively correlated with model size. Ni et al. [9] produced a digital coal model using CT scans combined with AVIZO image processing technology and simulated the flow process of coalbed methane in large pores, which revealed the distribution of pressure and the velocity field. Wang et al. [10] established a model using 6 coal samples, simulated the seepage conditions of coalbed methane under different pressure gradients, and found that the non-Darcy coefficient was negatively correlated with the effective porosity and permeability. Yu et al. [11] proposed using bitmap vectorization theory based on the reconstruction method of a three-dimensional, solid material structures model and simulated the uniaxial compression process. Sun et al. [12] obtained the samples of multicomponent, structural, and porosity values of cement through a three-dimensional reconstruction of CT images and discrete element modelling. Yuan [13] used a combination of X-ray computed microtomography, scanning electron microscopy, and mercury intrusion porosimetry to detect large-scale hydraulic conductivity changes in a wide range of sizes related to changes in the porous microstructural variations.

The advantages of three-dimensional modelling are clear, but the shortcomings are equally obvious, such as only being able to reflect two phases, primarily the rock skeleton and the void space [11, 14–16]. However, for a soil-rock mixture, models need to reflect the three phases of soil, block stone, and void space. At present, most seepage simulations of the soil-rock mixture are based on a two-dimensional artificial model [17–19], and the main simulation includes soil and rock as the two phases. Using a CT image with a two-dimensional model is proposed to reflect a realistic sample of a three-phase distribution. At the same time, a threshold control method is established for the soil-rock mixture, a multivariable model based on single model is developed, and the relationship between the mesoscopic structure and macroscopic permeability is explored. These studies provide guidance for the future development of laboratory tests.

2. Basic Principles of the Threshold Control Method

2.1. Preparation of Soil-Rock Mixture Specimen. The study was based on a single sample of a soil-rock mixture. The material properties of the laboratory specimens of soil and rock are shown in Table 1. In the sample preparation process, the materials are placed in a steel cylinder with a height of 160 mm and an inner diameter of 50 mm and then compressed. The initial height of the consolidated sample is approximately 130 mm, and the soil-stone mixture is formed under consolidation. The specimen size (φ) is 50×100 mm, the initial bulk material moisture content is 20%, and the maximum consolidation pressure is 2000 kPa, which simulates a buried depth of approximately 100 m (Figure 2).

2.2. Principles of Two-Dimensional Numerical Model Construction. CT image is a kind of digital image. If the research object is limited to the image changing at different times, the image intensity can be expressed as formula (1). In the formula, I is defined as the image intensity and (x, y) represents the plane coordinate of the image:

$$I = f(x, y). \tag{1}$$

According to Lambert-Beer's law [20], the intensity of X-ray penetrating the material is attenuated, and the relationship between the incident and outgoing X-ray intensity is shown in the following formula:

$$I = I_0 e^{-\mu \Delta x}, \tag{2}$$

where I_0 is the intensity of incident X-ray, I is the intensity of the outgoing X-ray, Δx is thickness, and μ is the linear attenuation coefficient of material. The linear attenuation coefficient of the material is related to its composition, density, and ray energy. The result of CT scan is the distribution image of X-ray attenuation coefficient within the detected specimen. The difference of X-ray attenuation coefficients of void, soil, and rock can be reflected as different grey values [21].

The grey value distribution in the image can be used to distinguish void space, soil, and rock. And, the greyscale value can be regarded as an intermediate variable, and porosity, which is associated with permeability, is assigned in the numerical model. We can therefore generate a numerical model that reflects the relationship between porosity and permeability.

In numerical models, porosity and permeability can be considered to be spatial point coordinates, which can be expressed as

$$\varphi(x, y) = \begin{cases} \eta_1 f(x, y), & 0 \le f(x, y) < I_1, \\ \eta_2 f(x, y), & I_1 \le f(x, y) < I_2, \\ \eta_3 f(x, y), & I_2 \le f(x, y) \le I_3, \end{cases} \tag{3}$$

where η_1, η_2, and η_3 reflect the void, soil, and rock block, respectively, and I_1, I_2, and I_3 are defined as the greyscale threshold values for the void, soil, and block, respectively. The representation of permeability is similar to these variable definitions.

If an appropriate threshold dividing point I_i is defined, we can use the numerical model and adjust the thresholds of the model accordingly.

However, in producing a numerical model that reflects actual samples, the greyscale images from CT scans reveal that the soil and stone mixture is highly heterogeneous. When we use CT technology to scan the reconstructed specimen, the continuity of grey values is better. However,

Table 1: Soil-rock mixture parameters.

Material	Type	Present (%)	Density (kg/m^3)	Moisture content (%)	Size
Soil	Clay	30	1750	20	Sifting 1 mm
Rock	Scree	70	2200	16	Sifting 8 mm

(a) (b) (c)

Figure 2: Sample preparation process.

different specimens have different greyscale values; we must therefore choose different methods to manage these differences. As seen in Figure 1, different greyscale values can be reflected clearly. The characteristics of the three kinds of media are shown in Figure 3, and the local, statistical results are shown in Figure 4.

From Figure 4, the greyscale of rock is mainly within the range of 130–255 and is concentrated within the range of 175–220. The soil gradation range corresponds to 115–255 and is concentrated within the range of 153–178. Pore space is in the gradation range of 0–102. The threshold between rock and soil is difficult to determine. Gradation ranges and the pores in rock and soil in this case tend to overlap, and the threshold range is between 102 and 115. Therefore, from the test, we cannot accurately define the soil and stone mixture distribution. However, as shown in Figure 5, a comparison of numerical modelling results and an actual specimen demonstrate that the threshold segmentation is accurate and within a certain range of error and therefore reflects the true three-phase distribution from analysed sections.

2.3. Threshold Control Method. As stated above, CT images of each point can be portrayed as a function of gradation values as shown in Figure 6. As seen from the image, the cumulative greyscale frequency of CT section images is the ratio of the greyscale pixel value to the total number of pixels in the section, which is the volume fraction of the phase, M_i, and can be expressed as

$$M_i = \sum_{0}^{i} \frac{n_k}{n}, \tag{4}$$

where k is the greyscale pixel value and n is the total number of pixels in the section.

The threshold method uses integration to control the gradation value, which reflects the proportions of the three phases. This method can generate multiple different models by dividing points along different thresholds.

3. Numerical Model of Soil-Rock Mixture

3.1. Select Threshold Control Points. To reflect the greyscale value distribution of the sample, 297 CT cross-sectional images of specimens for a total height of 100 mm were made to achieve a system closer to the actual specimen.

The CT scan energy was set to 150 kV, and the cross-sectional image obtained by the CT scan could clearly distinguish between macroporosity, soil, and stone. The colour depth of the selected CT image is 8 bit, and the greyscale value range is from 0 to 255 where 0 represents black and 255 represents white. An image statistics programme in MATLAB that can calculate greyscale values was used. The greyscale value versus the cumulative frequency of the greyscale value is shown in Figure 7.

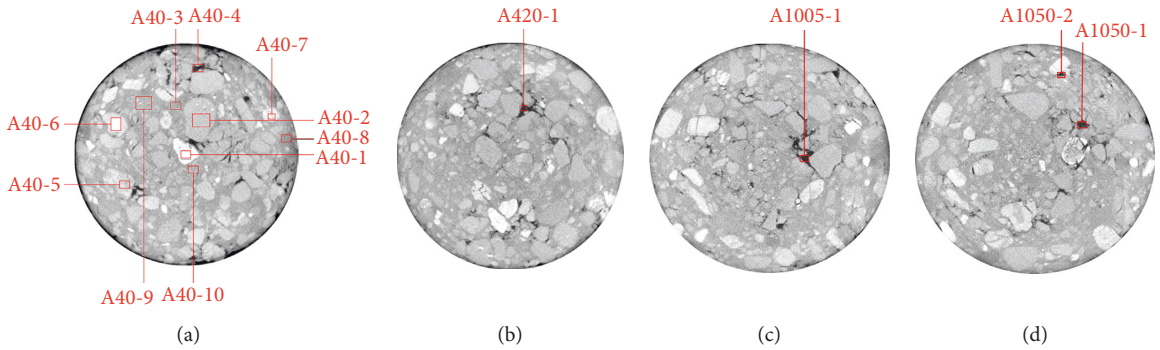

Figure 3: Greyscale value frequency of a local, statistical region.

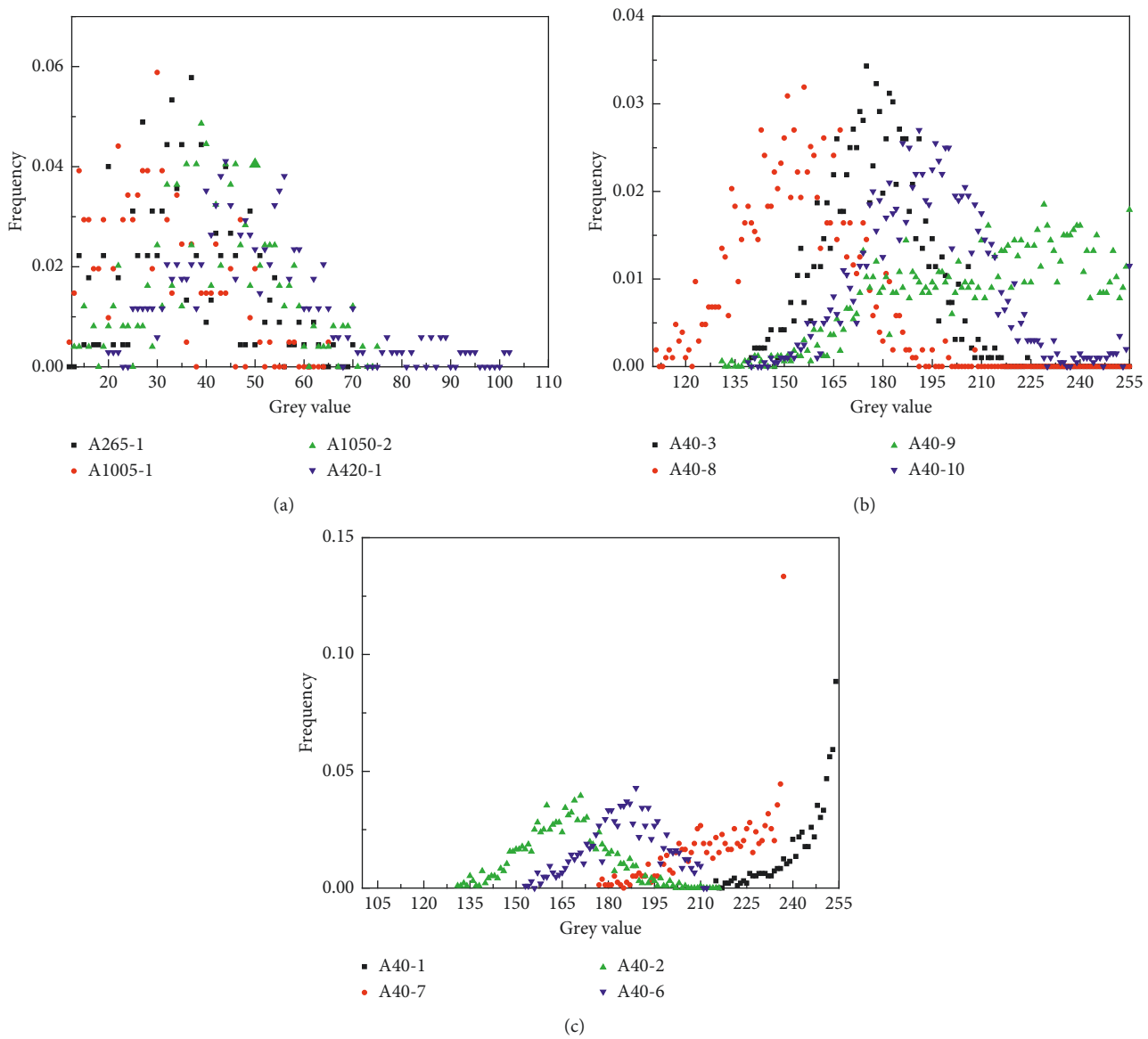

Figure 4: Greyscale value frequency statistics of (a) pores, (b) soils, and (c) block stone.

From Figure 7, two greyscale values can be arbitrarily selected that correspond to a mixture of the three media, and the difference in the corresponding function value is the volume fraction of that phase. For example, given greyscale values I and J ($i < j$), the proportion of space occupied by medium ij is expressed as $M_{i,j}$. If the maximum greyscale

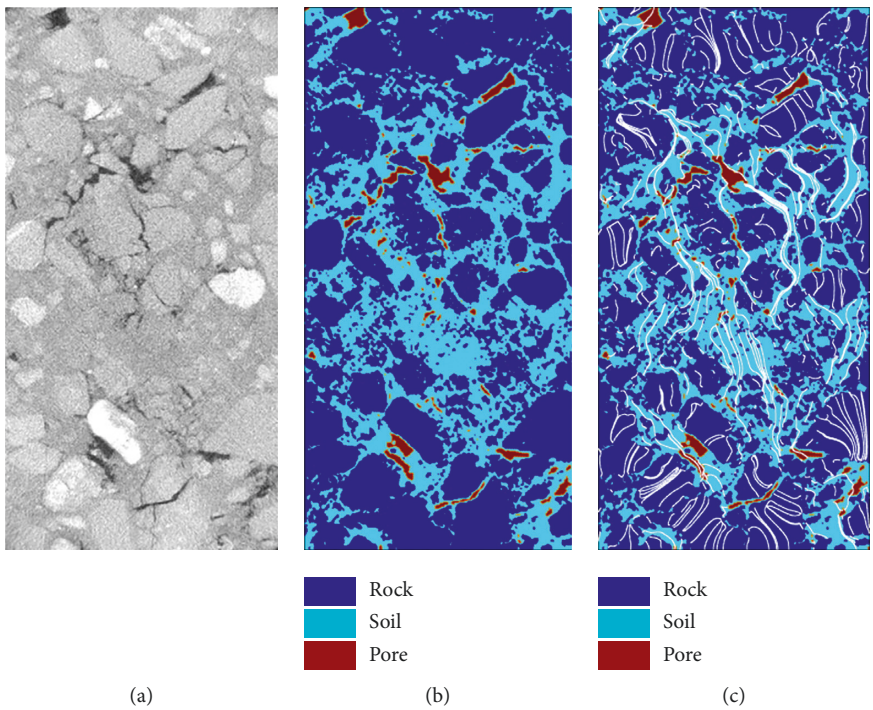

Figure 5: CT image cumulative greyscale value frequency statistics.

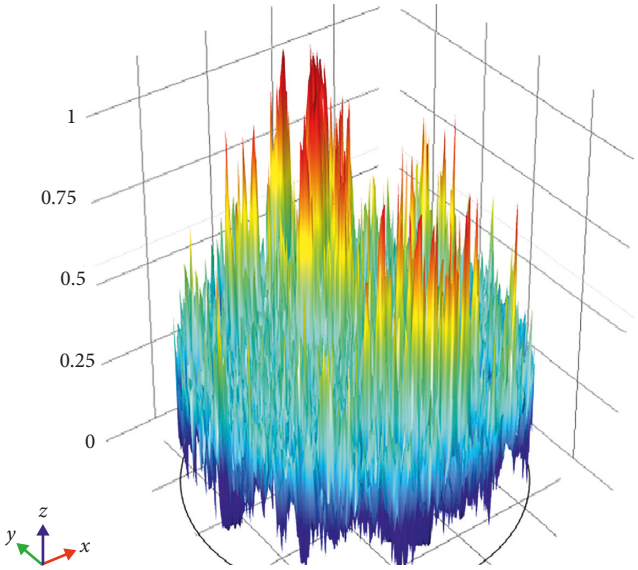

Figure 6: Greyscale value function image of soil-rock mixture.

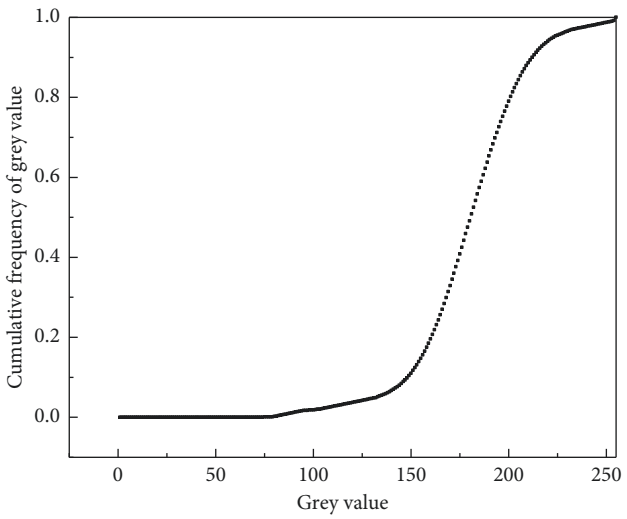

Figure 7: CT image cumulative greyscale value frequency statistics.

value is I, then $M_{0,i}$ represents macropores. This method can be used to find the threshold boundary points of the different volume fractions of the three phases.

3.2. Construction of the Permeability Parameters Model. We construct a permeability parameters model for soil-stone mixtures with mesoscopic characteristics in which permeability and porosity as a function of permeability characteristics are assigned spatial points. A mesoscopic visualization of the model structure offers a finer view of parameter assignments. The sample parameters of soil and rock mixture are shown in Table 2.

The calculation of permeability is based on Darcy's law and absolute permeability is adopted. The calculation is as follows:

$$K = \frac{Q\mu L}{\Delta P A}, \tag{5}$$

where A is rock cross-sectional area, μ is viscosity, L is length of rock, ΔP is rock pressure difference, and Q is flow per unit time. Q can be obtained by integrating the fluid velocity at the model outlet, as shown in the following equation:

Table 2: Different medium permeability parameters.

	Porosity	Soil	Rock
Poriness (a.u.)	1	0.4	0.1
Permeability (M^2)	1×10^{-4}	5×10^{-8}	1×10^{-12}

$$Q = \int v dx, \tag{6}$$

where v is the velocity at any point on the X-axis when the bottom of the model is the X-axis.

Threshold partitioning is used in modelling the sample. According to the three-phase greyscale value distribution obtained in section 2.2, the greyscale values 115 and 175 are used as the threshold partition points that coincide with the actual CT section. The finite element software was used to generate the model and simulate the seepage flow The numeric modelling results generated after parameter assignment are shown in Figure 5.

The size of the pores is reflected by the specimen's colour, and the white streamlines represent a Darcy flow field, which reflects the effluent and effluent velocity flowing around the specimen.

By comparing the model results to the original CT images, we can conclude that the threshold control method has a high likelihood of reducing errors. These results also demonstrate that applying thresholds to a section using multigradation value statistics is feasible and credible.

4. Mesoscopic Permeability Simulation Test

This numerical test is based on CT imaging and changing the proportions of macroscopic voids, soil, and rock through constant adjustments to the thresholds. The advantage of this approach is that even though the location of stone blocks may not be consistent for different rock contents of the specimens, we can ensure that the distribution of stone blocks in the specimen is unchanged. In addition, size of pores in soil and stone is generally small, and it can be different to distinguished in large-size CT scan. So, this article refers to macropore, and total porosity of the material n is calculated as follows.

In addition, the size of the pores in soil and stones is generally small and can therefore be difficult to distinguish in CT scans of larger objects. This study therefore focuses on macropores, and total porosity of material n can be calculated as follows:

$$n = \alpha n_a + \beta n_s + \gamma n_r, \tag{7}$$

where n_a is the macroscopic porosity of the air-filled sections, n_s is soil porosity, n_r is rock porosity, and α, β, and γ are weighted values, respectively, representing the proportion of space volume occupied by the pore, soil, and rock.

4.1. Impact of Macroporosity on Permeability at a Volume Fraction of 0.5. Five specimens were designed to research the effect of macroscopic porosity on permeability, as shown in Table 3. The threshold control points are selected according to Figure 4. The volume fraction of 5 selected specimens was maintained at 0.5 by adjusting the pore threshold, which increases the volume fraction of the macroscopic voids and is demonstrated in Figure 8. In the numerical simulation, we simulate a seepage scenario at a standard atmospheric pressure of 101 kPa and using Darcy's Law. The results are shown in Figure 9.

Table 3: A-1 to A-5 samples parameters.

Sample	Proportion (%)			Total porosity	Threshold value		
	Pore (α)	Earth (β)	Rock (γ)		Pore	Earth	Rock
A-1	0	0.5	0.5	0.25	0	181	255
A-2	0.1	0.4	0.5	0.31	148	181	255
A-3	0.2	0.3	0.5	0.37	161	181	255
A-4	0.3	0.2	0.5	0.43	169	181	255
A-5	0.4	0.1	0.5	0.49	175	181	255

The absolute permeability of the soil-rock mixture obtained by calculation is shown in Figure 10.

To demonstrate the increased reliability of the simulation results, we changed the pore threshold values from 148 to 175 and retained a soil threshold of 181. The results are shown in Figure 10. The labelled point is the result of 5 samples, A-1 to A-5. It can be seen from the figure that permeability increases with an increase in macroscopic porosity and total porosity. The specimen A-4 demonstrates the beginning of rapid permeability where the macroscopic porosity corresponds to 0.30, and total porosity is 0.43. The permeability of specimens A-1 and A-4 is very small with an average of 1.31×10^{-7}. The permeability of A-1 is the lowest of the specimens, and the permeability of pure soil is close to A-1. As shown in Figure 9, which depicts the flow fields, when the macroscopic porosity reaches 0.4 (A-5 specimen), the contrast to A-4 is noticeable based on the larger area of macroscopic void penetration, which makes permeability rise rapidly.

However, the actual sample with a pore volume fraction of 0.3 was a compacted specimen. The specimen with a high porosity is similar to the compacted specimen based on morphology and results. In general, it can be concluded that macroscopic voids that do not penetrate deeply into the mixture will increase the permeability of the soil-rock mixture, but the increase is not significant, whereas the permeability of the soil-rock mixture is greatly increased by high porosity. These results also demonstrate that this type of mixture has a water-retaining effect that can ensure humus will not be lost even with underground infiltration.

4.2. Impact of Macroporosity on Permeability at a Volume Fraction of 0.2. This section will maintain the macroscopic volume fraction of 0.2 by changing the soil threshold value. The parameters corresponding to samples A-6 to A-10 are shown in Table 4, and numerical modelling and simulation results are shown in Figures 11–13.

With the first set of tests, the curves shown in Figure 13 are the simulated results where the earth threshold value changes from 169 to 194. The pore threshold value of 161 is

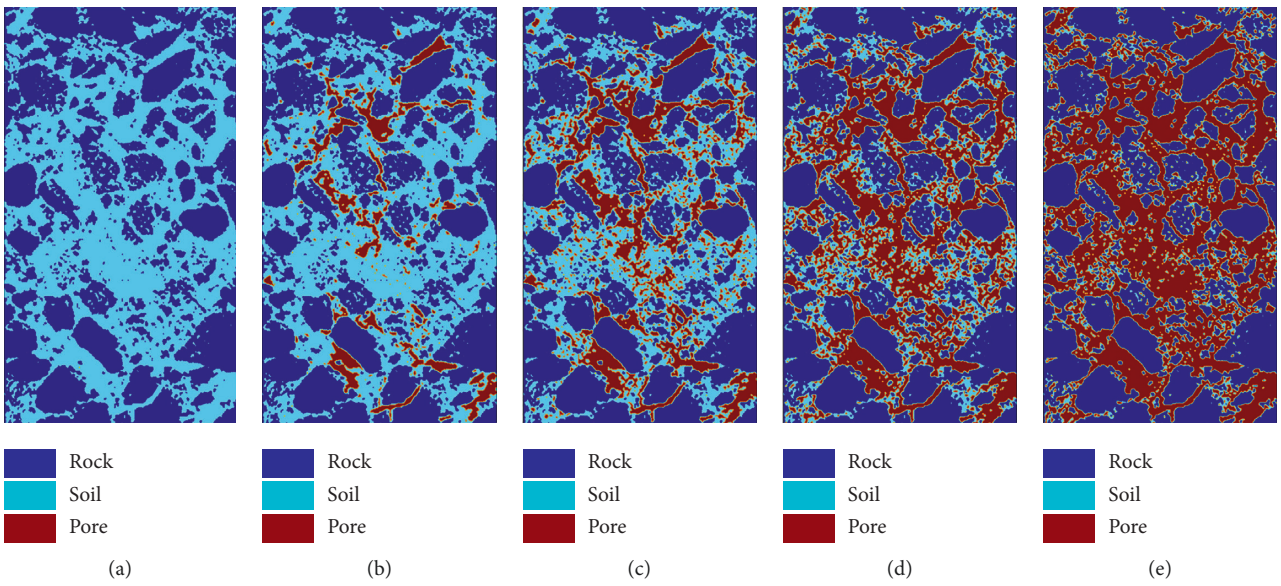

Figure 8: Numerical model of A-1 to A-5 samples.

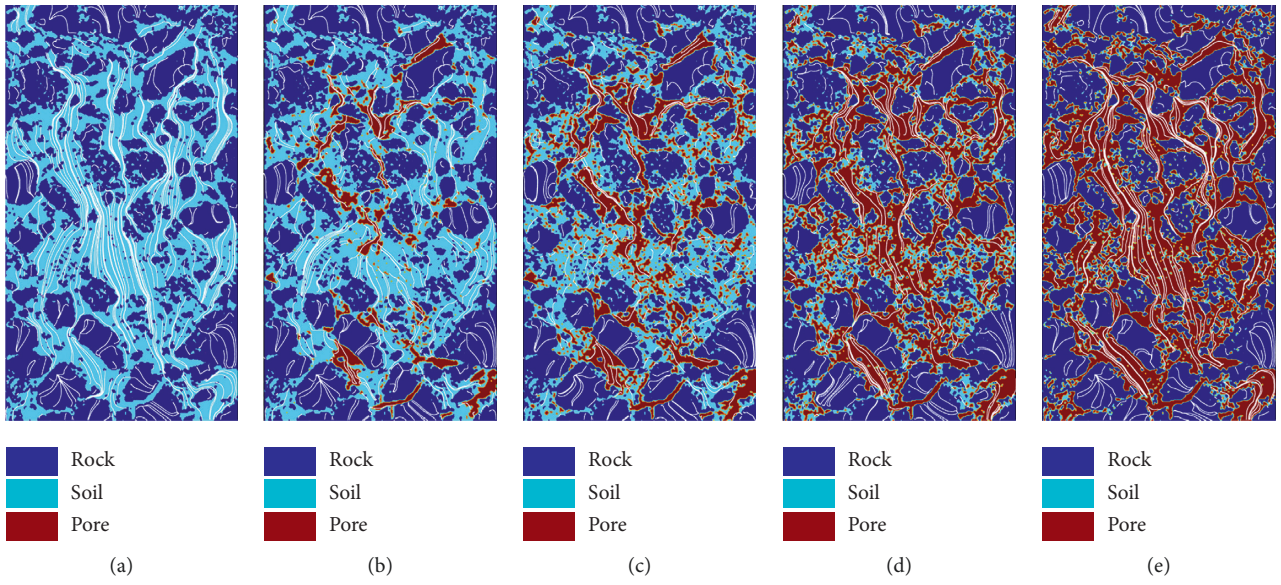

Figure 9: Seepage simulation results of A-1 to A-5 samples.

maintained across all specimens. As seen from Figure 13, at a stone content of 0.5 (A-8), the model point of view is the soil or rock mass. The permeability of A-6 is 5.86×10^{-9}, and the permeability of A-10 is 1.77×10^{-6}, which means the permeability of A-6 is between the values corresponding to rock and pore space, and the permeability of A-10 is between the values corresponding to pore space and soil. As shown in Figure 12, the velocity streamlines of A-6 and A-7 are concentrated around the rock blocks, which directly reflect the influence of the rock material. The corresponding diagrams for A-9 and A-10 mainly depict soil. In general, increases in stone material will reduce the permeability of the soil-rock mixture, and the permeability will reduce with an increase in the stone material. In other words, the higher the amount of stone in soil humus, the better the water retention.

5. Conclusion

Soil-stone mixtures, which can be a highly heterogeneous and nonuniform medium, can demonstrate the same macroscopic parameters but may not produce two pieces of the same mesoscopic structure within the same specimen. In this paper, mesoscopic numerical modelling based on the threshold control method provides an effective method for describing the mesoscopic characteristics of soil-rock mixtures. The results are as follows:

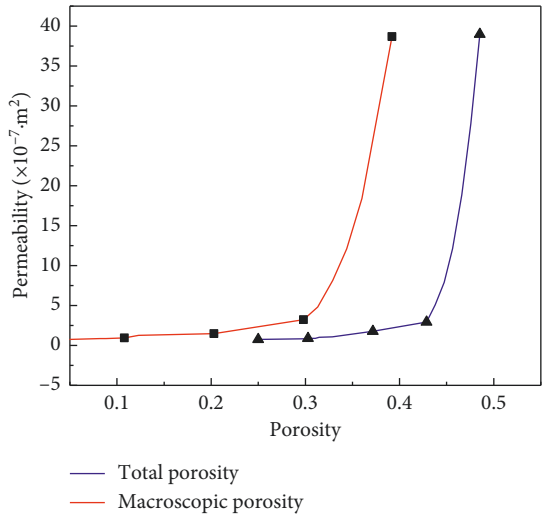

Figure 10: Permeability curve of A-1 to A-5 samples.

Table 4: A-6 to A-10 sample parameters.

Sample	Proportion (%)			Total porosity	Threshold value		
	Pore (α)	Earth (β)	Rock (γ)		Pore	Earth	Rock
A-6	0.2	0.1	0.7	0.31	161	169	255
A-7	0.2	0.2	0.6	0.34	161	175	255
A-8	0.2	0.3	0.5	0.37	161	181	255
A-9	0.2	0.4	0.4	0.4	161	187	255
A-10	0.2	0.5	0.3	0.43	161	194	255

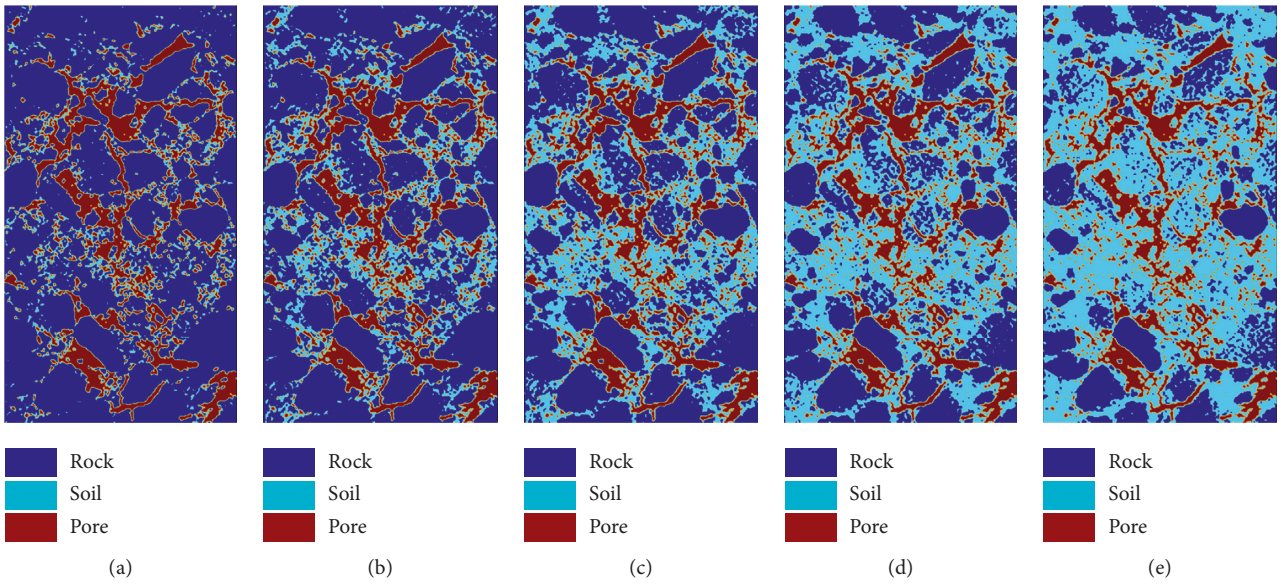

Figure 11: Numerical model of A-6 to A-10 samples.

(1) Statistics calculated from the partial CT sections can provide a comparison between the numerical model and the actual sample picture. The results prove the rationality and feasibility of this method in describing the three phases are included in the soil-stone mixture.

(2) Based on statistics of soil-rock specimen with a size of 100 mm × 50 mm and using 297 CT scans, we can obtain cumulative greyscale value frequencies and the threshold segmentation boundaries, which can accurately describe volume fractions of the three phases that exist in the soil-rock mixture.

(3) The effect of macroscopic porosity and rock content on permeability was studied by using the threshold control method based on the mesoscopic numerical

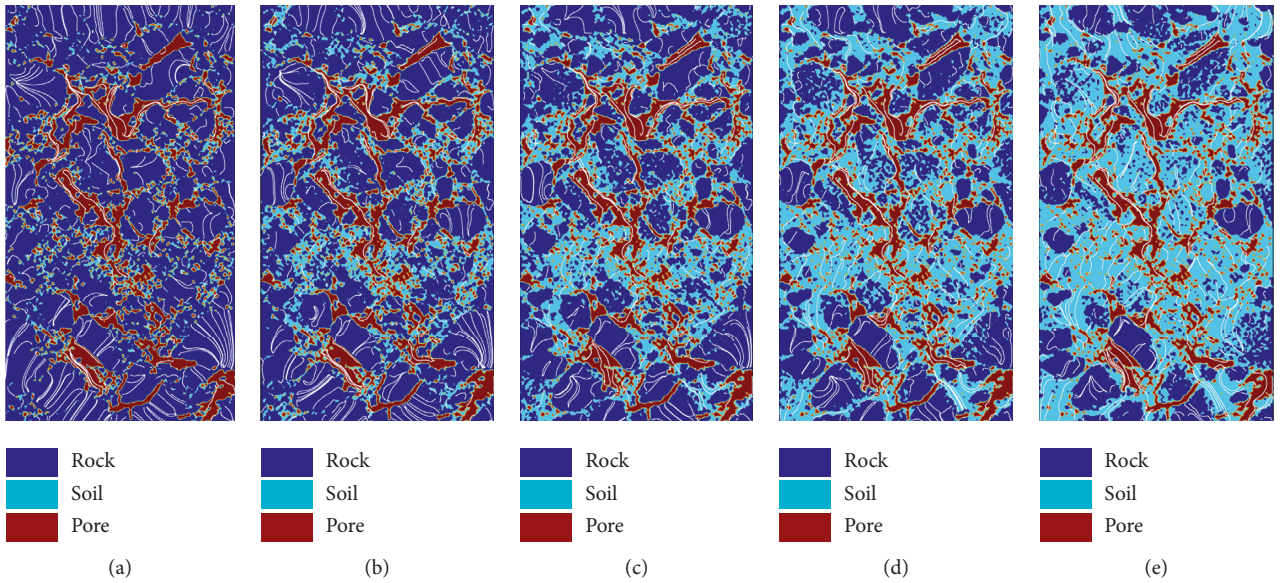

Figure 12: Seepage simulation results of A-6 to A-10 samples.

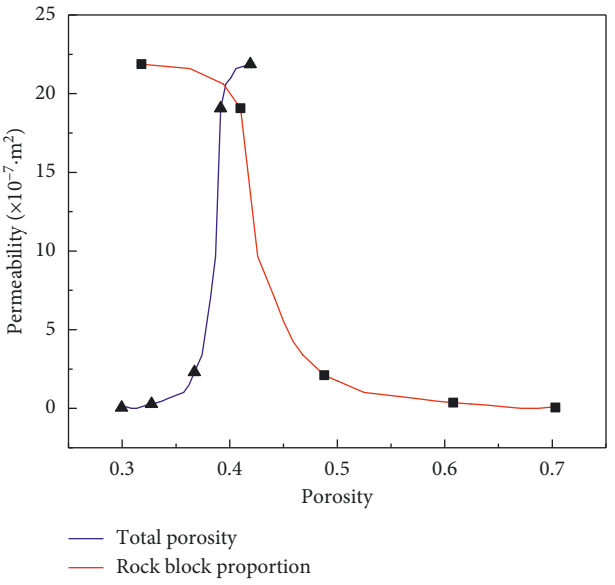

Figure 13: Permeability curve of A-6 to A-10 samples.

model, and the error caused by different space distributions within specimens was avoided in the laboratory. By analysing the permeability curves and streamlines in a flow field, we conclude that macroscopic voids that do not penetrate deeply into the mixture will increase the permeability of the soil-rock mixture, but the increase is not significant, whereas the permeability of the soil-rock mixture is greatly increased by high porosity, and the permeability of the soil-rock mixture will be closer to the rock skeleton with an increase in rock block proportions.

(4) In reclamation projects, the rock content should be increased to ensure lower permeability and better water retention.

(5) The mesoscopic numerical method based on the threshold control method can establish specific models for the experiment. If combined with a reasonable simulation algorithm, the method can obtain credible simulation test results, which will provide reliable guidance for future testing.

(6) The advantage of threshold control method is to identify the soil, rock, and pore of the specimen, and it can be used to establish a three-dimensional model containing pore information in future studies, instead of the traditional model with only soil and rock. And, more precise simulation tests can be conducted.

Data Availability

The data used to support the findings of this study are included within the article.

Conflicts of Interest

The authors declare that there are no conflicts of interest regarding the publication of this article.

Acknowledgments

This study was supported by the National Natural Science Foundation of China (Grant nos. 51804299 and 51574222) and the Natural Science Foundation of Jiangsu Province, China (Grant no. BK20180646).

References

[1] L. Zhu, "Reclamation scheme and benefit analysis of Anjialing open-pit mine dump," *Opencast Mining Technology*, vol. 32, no. 5, pp. 74–76, 2017.

[2] Z. Z. Han, "Ecological environment restoration measure in Ha'erwusu open-pit coal mine," *Opencast Mining Technology*, vol. 31, no. S1, pp. 72–74, 2016.

[3] J. Fu, "Study on land reclamation technology in the open-pit mine dump of Shengli mining area," *Opencast Mining Technology*, vol. 32, no. 2, pp. 84–87, 2017.

[4] W. C. Li, J. Li, X. Y. Li, X. X. Wang, and S. P. Lv, "Research on reclamation greening technology in Yimin open-pit mine," *Opencast Mining Technology*, vol. 31, no. 6, pp. 94–96, 2016.

[5] L. Chen, P. Zhang, and H. Zheng, "Mesostructure modeling of soil -rock mixtures and study of its mesostructural mechanics based on numerical manifold method," *Rock and Soil Mechanics*, vol. 38, no. 8, pp. 2402–2410, 2017.

[6] W. J. Xu and S. Wang, "Meso-mechanics of soil-rock mixture with real shape of rock blocks based on 3D numerical direct shear test," *Chinese Journal of Rock Mechanics and Engineering*, vol. 35, no. 10, pp. 2152–2160, 2016.

[7] Q. L. Liao, X. Li, W. C. Zhu, and J. S. Liu, "Structure model construction of rock and soil aggregate based on digital image technology and its numerical simulation on mechanical structure effects," *Chinese Journal of Rock Mechanics and Engineering*, vol. 29, pp. 155–162, 2010.

[8] Q. X. Meng, H. L. Wang, W. Y. Xu, and M. Cai, "A numerical homogenization study of the elastic property of a soil-rock mixture using random mesostructure generation," *Computers and Geotechnics*, vol. 98, pp. 48–57, 2018.

[9] X. Ni, J. Miao, R. Lv, and X. Lin, "Quantitative 3D spatial characterization and flow simulation of coal macropores based on μCT technology," *Fuel*, vol. 200, pp. 199–207, 2017.

[10] G. Wang, X. X. Yang, X. Q. Zhang, M. M. Wu, and W. X. Li, "Numerical simulation on non-Darcy seepage of CBM by means of 3D reconstruction based on computed tomography," *Journal of China Coal Society*, vol. 41, no. 4, pp. 931–940, 2016.

[11] Q. L. Yu, T. H. Yang, S. B. Tang et al., "The 3D reconstruction method for quasi-brittle material structure and application," *Engineering Mechanics*, vol. 11, pp. 51–62, 2015.

[12] W. Sun, K. Hou, Z. Yang, and Y. Wen, "X-ray CT three-dimensional reconstruction and discrete element analysis of the cement paste backfill pore structure under uniaxial compression," *Construction and Building Materials*, vol. 138, pp. 69–78, 2017.

[13] Z. X. Yuan, *Damage Evolution and Numerical Simulation of Concrete Based on Computer Tomography Images*, China University of Mining & Technology, Beijing, China, 2016.

[14] G. Dalla Santa, S. Cola, M. Secco, F. Tateo, R. Sassi, and A. Galgaro, "Multiscale analysis of freeze-thaw effects induced by ground heat exchangers on permeability of silty clays," *Géotechnique*, vol. 69, no. 2, pp. 95–105, 2019.

[15] H. F. Sun, Y. Ju, M. X. Xing, X. F. Wang, and Y. M. Yang, "3D identification and analysis of fracture and damage in soil-rock mixtures based on CT image processing," *Journal of China Coal Society*, vol. 39, no. 3, pp. 452–459, 2014.

[16] G. Wang, X. X. Yang, X. Q. Zhang, W. X. Li, and L. K. Shi, "Numerical simulation of gas flow in pores and fissures of coal based on segmentation of DTM threshold," *Chinese Journal of Rock Mechanics and Engineering*, vol. 35, no. 1, pp. 119–129, 2016.

[17] X. L. Ding, H. M. Zhang, S. L. Huang, B. Lu, and Q. Zhang, "Research on mechanical characteristics of unsaturated soil-rock mixture based on numerical experiments of meso-structure," *Chinese Journal of Rock Mechanics and Engineering*, vol. 31, no. 8, pp. 1553–1566, 2012.

[18] H. Shen, X. Q. Luo, and J. F. Bi, "Numerical simulation of internal erosion characteristics of block in matrix soil aggregate," *Rock and Soil Mechanics*, vol. 38, no. 5, pp. 1497–1502, 2017.

[19] W. J. Xu and Y. G. Wang, "Meso-structural permeability of S-RM based on numerical tests," *Chinese Journal of Geotechnical Engineering*, vol. 32, no. 4, pp. 542–550, 2010.

[20] G. T. Herman, *Image Reconstruction from Projects: The Foundation of Computerized Tomography*, Academic Press, Cambridge, MA, USA, 1980.

[21] Y. Wang, X. Li, J. M. Jue et al., "Calculation and application of porosity based on gray level of CT image," *Journal of Hydraulic Engineering*, vol. 46, no. 3, pp. 357–365, 2015.